Surface Science 732 (2023) 122283

Contents lists available at ScienceDirect

Surface Science

journal homepage: www.elsevier.com/locate/susc

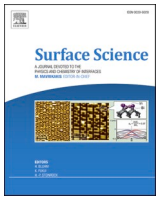

Functionalized silica nanoparticles within a multicomponent oil emulsion by molecular dynamic study

Lucas S. de Lara [a,e,*], Vagner A. Rigo [b,e,*], Taiza A.S. do Carmo [c], Caetano R. Miranda [d,e,*]

[a] Departamento de Física, Universidade Estadual de Ponta Grossa (UEPG), Ponta Grossa, PR, Brazil
[b] Universidade Tecnológica Federal do Paraná (UTFPR), Cornélio Procópio, PR, Brazil
[c] Instituto de Física, Universidade de São Paulo (IF-USP), São Paulo, SP, Brazil
[d] Universidade Tecnológica Federal do Paraná (UTFPR), Ponta Grossa, PR, Brazil
[e] Centro de Ciências Naturais e Humanas (CCNH), Universidade Federal do ABC (UFABC), Santo André, SP, Brazil

A B S T R A C T

Molecular dynamics simulations were employed to study hydroxylated and functionalized SiO_2 nanoparticles (NPs) within a light crude oil under different temperatures. The model oil comprised a combination of aromatics, alkanes, and cycloalkanes, while the hydroxylation, PEGlyation, and sulfonation of the NPs were evaluated. The effects of functional size were considered for PEGlyated NPs. Interestingly, benzene clusters dispersed in the oil phase were formed for all systems studied; clusters of 9 and 11 molecules were the most common. The benzene clusters adsorbed onto the NPs, forming a surrounding shell approximately 10 Å in width. The agglomeration of aromatic molecules was more evident for hydroxylation covering: the density of benzene molecules in the first shell of aromatic molecules surrounding the NPs decreased in the order NP-H, NP-SA, NP-EG, and NP-PEG2 and reached a maximum for hydroxylated NPs, where the hydrocarbons form a first shell of molecules ~25 Å in width. The density of benzenes is 24% greater than in pristine oil. Compared to other coverings, this effect reduces the NP–oil interfacial tension for the hydroxylated NPs by about 15%. Our results indicated that the adsorption of benzene on NPs and the NPs–oil interfacial tension could be tuned by the NP covering. This degree of control is highly desirable for applications of NPs in enhanced oil recovery processes.

1. Introduction

Among nanostructured materials, silica nanoparticles have been widely used in surface engineering, energy, and bio applications. In particular, NPs are often used in the biomedical sector as a drug delivery vehicle [1,2] for vaccines [3]. In surface design, they have been used to develop surfaces with hydrophobic [4] and tribologic [5] properties, and more recently as an agent to tune the interfacial properties of liquids [6–11]. This kind of information is valuable to the oil industry, where nanoparticles can potentially be used for enhanced oil recovery (EOR) [10–12] and the mitigation of oil spills [13]. The broad applicability of NPs is a function of their biocompatible properties, a controllable and accessible surface chemistry, and their relatively low cost [14].

For most applications, NPs must be dispersed in a fluid medium. This is the case for EOR and oil spill mitigation, where oil and brine are the most common fluid media. Salt ions can accumulate on the surface of NPs dispersed in brine, which alters their suspension stability [8,9,11,12]. The adsorption of ions on the silica surface and the formation of charged layers surrounding NPs have been the subject of many publications [8–10,15–17]. A literature review also demonstrated that the accumulation of water molecules [18] and salt ions [9,10] occurs in NPs functionalized by hydrophobic and hydrophilic molecules [9–11,18], where these surface groups aid the stabilization of the NP suspension [19,20].

Although dispersions of NPs in water and brine are well-studied, the properties of these nanoparticles when dispersed in oil have received less attention, despite their importance to EOR applications [10–12]. The interaction of hydrocarbons with a silica surface has been studied using molecular dynamics, and the results indicated that the aromatic molecules were adsorbed on silica surfaces [21,22]. They also showed that the molecule–surface interaction mechanism occurred through weak van der Waals coupling between the molecular aromatic ring and the hydroxyl groups on the silica surface. Through simulations [23] and experiments [24], the interaction of alkane molecules and NPs was studied using decane as a single oil component. In a more recent study [10], we examined surface-modified NPs at the oil–brine interface, where the light oil was modeled using a realistic combination of aromatic, alkane, and cycloalkane molecules, and found that benzenes accumulated on the silica surface, even on the NPs in the brine phase.

Additionally, aromatic molecules can agglomerate within crude oil even without chemical additives (molecules or nanoparticles) [25]. Benzene, in particular, is subject to agglomeration, which results in

* Corresponding authors.
E-mail addresses: lslara@uepg.br (L.S. de Lara), vagnerrigo@utfpr.edu.br (V.A. Rigo), crmiranda@usp.br (C.R. Miranda).

https://doi.org/10.1016/j.susc.2023.122283
Received 1 January 2023; Received in revised form 25 February 2023; Accepted 1 March 2023
Available online 8 March 2023
0039-6028/Published by Elsevier B.V.

nanoclusters that have specific magic numbers of molecules [26–28]. *Ab initio* and molecular dynamics simulations agree that benzene clusters with 13 molecules are the most stable [26,28]. This value is consistent with recent nuclear magnetic resonance (NMR) experiments performed on fossil fuel samples [25]. From those results, the aromatic molecules are expected to adsorb on NPs when dispersed in a crude oil emulsion. Moreover, the interaction between NPs and benzene clusters and their potential effects have never been properly examined.

For multicomponent oil systems, knowledge of the molecular adsorption processes on NPs and how these processes affect the interfacial and diffusion properties of each oil component is essential. Accordingly, the characterization and manipulation of these properties are key points for potential applications in the oil industry. For example, higher nanoparticle mobility and reduced oil–nanofluid interfacial tension can improve oil recovery through the structural disjoining pressure mechanism, as suggested by Wasan *et al.* [12,29]. This process uses NPs suspended in a fluid (nanofluid) to detach oil drops from a surface. In essence, the structure of NPs in the oil–brine surface contact line generates an increase in the local pressure gradient, which increases as the NP concentration increases, which results in a spreading force. In this aspect, the knowledge of NP–oil interfacial tension is essential for selecting nanofluids that provide a lower oil–nanofluid interfacial tension. Considering the importance of oil-dispersed NPs for technological and scientific applications, more detailed knowledge of such systems is highly desirable.

In this study, we used classical molecular dynamics to investigate the interaction of NPs with the hydrocarbon molecules present in light crude oil [30]. In addition to hydroxylated nanoparticles, NPs functionalized with hydrophilic and hydrophobic groups were considered. The formation and agglomeration of molecular clusters on NPs were monitored by density profiles, while the interfacial, transport, and structural properties were determined for the NP–oil interface.

2. Materials and methods

The computational model for crude light oil [30] incorporates a combination of eight hydrocarbon molecules, including alkanes and aromatics. The model for alkanes contains a total of 501 (0.14 wt), 458 (0.12 wt), 543 (0.15 wt), 537 (0.14 wt), 334 (0.09 wt), and 543 (0.15 wt) molecules of hexane, heptane, octane, nonane, cyclohexane, and cycloheptane, respectively. The aromatics include 543 (0.15 wt) and 209 (0.06 wt) molecules of toluene and benzene, respectively. This model is a standard way to study light oil (~ 0.89 g/cm^3), and is widely found in the literature [6,10,31].

The NPs are generated using a previously employed procedure [18]. Based on experiments [32,33] and theoretical considerations [18,33], the hydroxylated NPs (NP-H) models have a diameter of 3 nm with silanol and germinal surface sites. Taking hydrophilicity variation into account, surface functionalization of NPs by polyethylene glycol and sulphonic (NP-SA) groups are considered for hydrophilic to hydrophobic, respectively. The grafting process inserts $Si(OH)_3$-$(CH_2)_3$-SO_3H (SA) and $Si(OH)_3$-$(CH_2$-CH_2-O)n-H (PEG) molecular groups onto the NP surface, based on the optimized process described in Ref. [18]. For PEGylated nanoparticles, chains with n = 1 and 2 ethylene glycol monomers are evaluated (EG and PEG2).

Molecular dynamics simulations are conducted by using the LAMMPS package [34]. The CHARMM-based force field is adopted to describe the molecular interactions for oil [35] and silica NPs [36]. The simulations are initially set in a cubic box with 10 nm inside, under periodic boundary conditions. For long-range electrostatic interactions, the reciprocal space Particle Particle Particle-Mesh (PPPM) method [34–37] is adopted, and a cutoff of 10 Å is used for van der Waals interactions. For each NPs-oil system, the simulations equilibrate 1.0 ps in NVE, 10.0 ps in NVT and 60.0 ns in NPT ensemble, with a time-step of 0.5 fs. The production is carried out in NVT, along 4.0 ns. Temperature and pressure are controlled by the Nosé-Hoover thermostat [38,39] and the Andersen barostat [40], respectively.

To obtain information regarding the distribution of oil components surrounding the NPs, radial density profiles *d(r)* are determined for each oil component. The *d(r)* is determined by taking the average components for infinitesimal shells around the center of NPs. For the interfacial tension properties of spherical symmetry, the Gibbs formulation is adopted to describe the interface tension in terms of the pressure tensor [41–43]:

$$\gamma = \left[-\frac{\left(P_l - P_g\right)^2}{8} \int_0^\infty r^3 \frac{dP_N(r)}{dr} dr \right]^{1/3} \quad (1)$$

where P_l and P_g represent the internal and external pressures acting on the NP, respectively, and $P_N(r)$ is the normal component of pressure

$$P_N(r) = \frac{2}{r^2} \int_0^r P_T(r) dr \quad (2)$$

where $P_T(r)$ is the tangential component of the pressure tensor. Pressure tensor values are obtained during the production phase at intervals of 1.0 ps for all atoms yielding 4000 blocks of data used in the interfacial tension calculation. In this case the error associated with all measures were on the order of 10^{-4} N/m.

The self-diffusion coefficient is determined through the slope of the mean square displacement (MSD(t) = $\langle |r_i(t) - r_i(0)|^2 \rangle$) in the Einstein equation:

$$D = \frac{1}{6} \lim_{t \to \infty} \frac{1}{N} \sum_{i=1}^{N} \frac{\mathrm{MSD(t)}}{t}. \quad (3)$$

3. Results and discussion

3.1. Structural properties

Figure 1a and b show the radial density profile *d(r)* of the NP-H surface at 300 and 350 K, respectively. As a general observation, aromatic molecules accumulate on the NP-H surface at both temperatures. However, the adsorption of aromatic molecules on the NP-H surface at 350 K (Fig. 1b) is lower than at 300 K (Fig. 1a). Additionally, the peak corresponding to the greatest density of cycloalkanes is further (27.5 Å) from the NP-H surface at 350 K compared to 300 K (19.0 Å). These results can be understood in terms of the greater thermal diffusion at 350 K. As both temperatures show similar results, the radial distribution function *g(r)* is calculated for 300 and 350 K (Supplementary Fig. S1).

—To access the preferential location and orientation of the molecules surrounding the NP-H surface, radial pair distribution *g(r)* curves are calculated between the carbon atoms in the hydrocarbon molecules and the H-atoms on the NP-H surface. The results for all molecules show that benzene and (a lesser amount of) cycloheptane agglomerate on the NP-H surface. For other hydrocarbons, only heptane, hexane, and octane show layered structures, albeit less developed than those of benzene. Their *g(r)* are presented in Supplementary Figs. S2 to S4. These results are consistent with those reported for a silica surface, where the adsorption of aromatic molecules is more favorable than alkane molecules [21]. Fig. 1c shows the results for benzene, where the first *g(r)* peak between the C-H pair of atoms indicates a benzene–surface distance of 2.34 Å. This distance is compatible with a planar configuration of molecules (the aromatic ring is parallel to the NP-H surface), consistent with previous results for these molecules surrounding the surface of a silica nanopore [44]. Fig. 1d shows the *g(r)* for cycloheptane molecules and surface H-atoms. The curve indicates that molecules form an ordered layer at 2.61 Å around the NP-H surface. The *g*® shows a second peak at ~4.00 Å, suggesting that the cycloheptanes form a second solvation shell surrounding the NP-H.

Figure 2a and b show the *d(r)* results for NP-SA–oil interfaces at 300

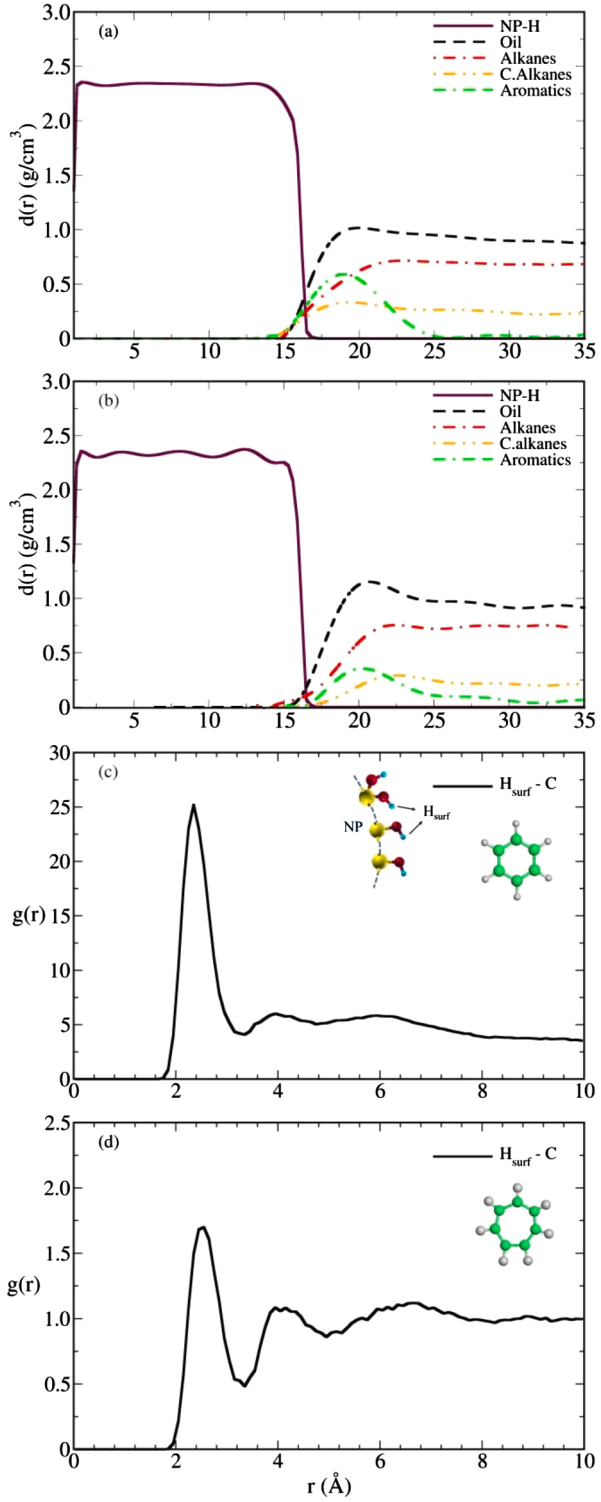

Fig. 1. Density profile of hydrocarbons surrounding the NP-H, as a function of the radial distance from the NP-H center of mass in (a) and (b), at 300 K and 350 K, respectively, while (c) and (d) show the radial pair distribution between surface H-atoms in nanoparticle and carbon atoms in benzene and cycloheptane molecules, respectively, at 300 K.

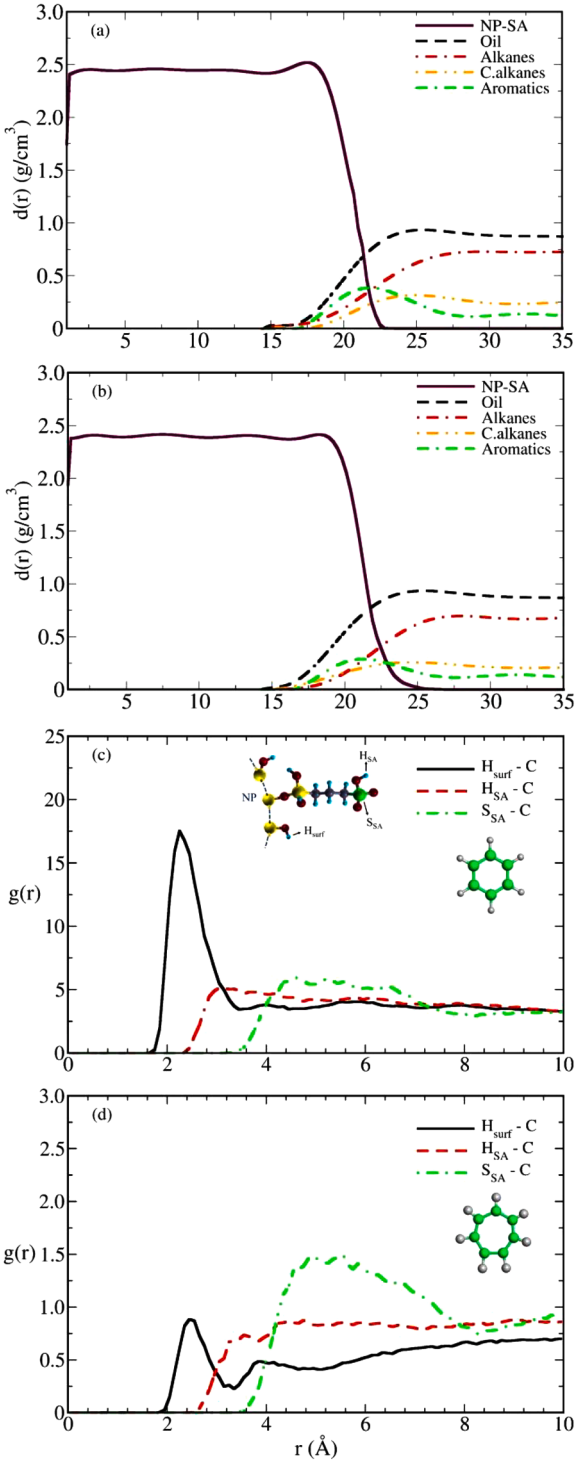

Fig. 2. Density profiles of hydrocarbons surrounding the NP-SA, as a function of the radial distance from the NP-H center of mass in graphs (a) and (b), at 300 K and 350 K, respectively. Graphs (c) and (d) give the radial pair distribution between selected atoms in nanoparticle (see inset) and carbon atoms in benzene and cycloheptane molecules, respectively, at 300 K.

and 350 K, respectively. These systems also show an accumulation of aromatic molecules on the NP surface (similar to the NP-H–oil interfaces in Fig. 1a and b). However, the degree of accumulation on the NP-SA surface is reduced compared to that on the NP-H surface under the same conditions. When compared to the NP-H (Fig. 1), the NP-SA (Fig. 2) has a larger radius due to the functional groups attached to the surface. As a result, at 300 and 350 K, the NP-SA has average radii of 22.5 and 25.0 Å, respectively. Fig. 2a and b also show that a greater accumulation of aromatic molecules occurs at approximately 22.0 and 21.5 Å for 300 and 350 K, respectively. This indicates that aromatic molecules accumulate only on the NP surface and not on the sulfonic

groups. As such, aromatic molecules accommodate themselves between the functional groups.

Fig. 2c shows the *g(r)* between the carbon atoms in benzene and selected atoms on the NP surface. The *g(r)* between the carbons and the surface H-atoms for NP-SA is slightly broader than that of NP-H (Fig. 1c), indicating the loss of the shell structure in NP-SA–oil. The *g(r)* between carbon atoms and the sulfur (S_{SA}) and hydrogen (H_{SA}) atoms in the functional group does not show a clear peak, suggesting there is no preferential position for benzene rings with respect to the functional groups. Similar behavior is seen with cycloheptane, as shown in Fig. 2d. However, the solvation layers surrounding the surface H-atoms are still present, although with lower intensity compared to the NP-H (Fig. 1d). As the other hydrocarbons do not demonstrate a significant accumulation on NP-SA, their *g(r)* are not shown.

Figure 3a-c show the *d(r)* and *g(r)* between NP-benzene and NP-cycloheptane for NP-EG–oil at 300 K, while Figs. 3d-f show similar results for the NP-PEG2–oil interfaces. The intensity of the *d(r)* peak for aromatic molecules on NP-EG (Fig. 3a) is slightly higher than that for NP-PEG2 (Fig. 3d); however, the accumulation of such molecules on NP-PEG2 is broader than that of NP-EG. Another interesting result is that the peak in *d(r)* for cycloalkanes and aromatic molecules occurs between functional groups for NP-PEG2. This indicates that cycloalkanes and aromatic molecules are also adsorbed on the surface sites. The findings for 350 K show the same trend as that of the NP-H and NP-SA systems (Supplementary Fig. S1).

The *g(r)* between the carbon atoms in benzene molecules and selected atoms in NP-EG (Fig. 3b) and NP-PEG2 (Fig. 3e) show that the first *g(r)* peak between benzene and the surface H-atoms of the NP occurs at 2.31 Å. The intensity of these *g(r)* peaks is lower than that for NP-H (Fig. 1c) and NP-SA (Fig. 2c). For cycloheptane molecules on NP-EG, Fig. 3c shows two solvation shells at 2.55 and 3.89 Å, where the first peak is less pronounced than the second. For NP-PEG2 (Fig. 3f), similar peaks appear at 2.39 and 3.87 Å, showing lower intensity than NP-EG. This suggests that a larger number of CH_3 spacers in PEG2 reduces the accumulation of such molecules on NP-PEG2 compared to NP-EG. The *g(r)* for other hydrocarbons in the oil do not present significant results, so they are not shown here.

To better describe and analyze the accumulation of aromatic molecules on the surface of NPs, Fig. 4a, b, c, and d present the time-averaged distributions of the benzene and toluene molecules in NP-H–oil, NP-SA–oil, NP-EG–oil, and NP-PEG2–oil interfaces, respectively. The results provide a visualization of the accumulation of aromatic molecules on NPs. All samples show the accumulation of benzenes on the NP surface and the formation of benzene clusters in solution. As expected from the *d*

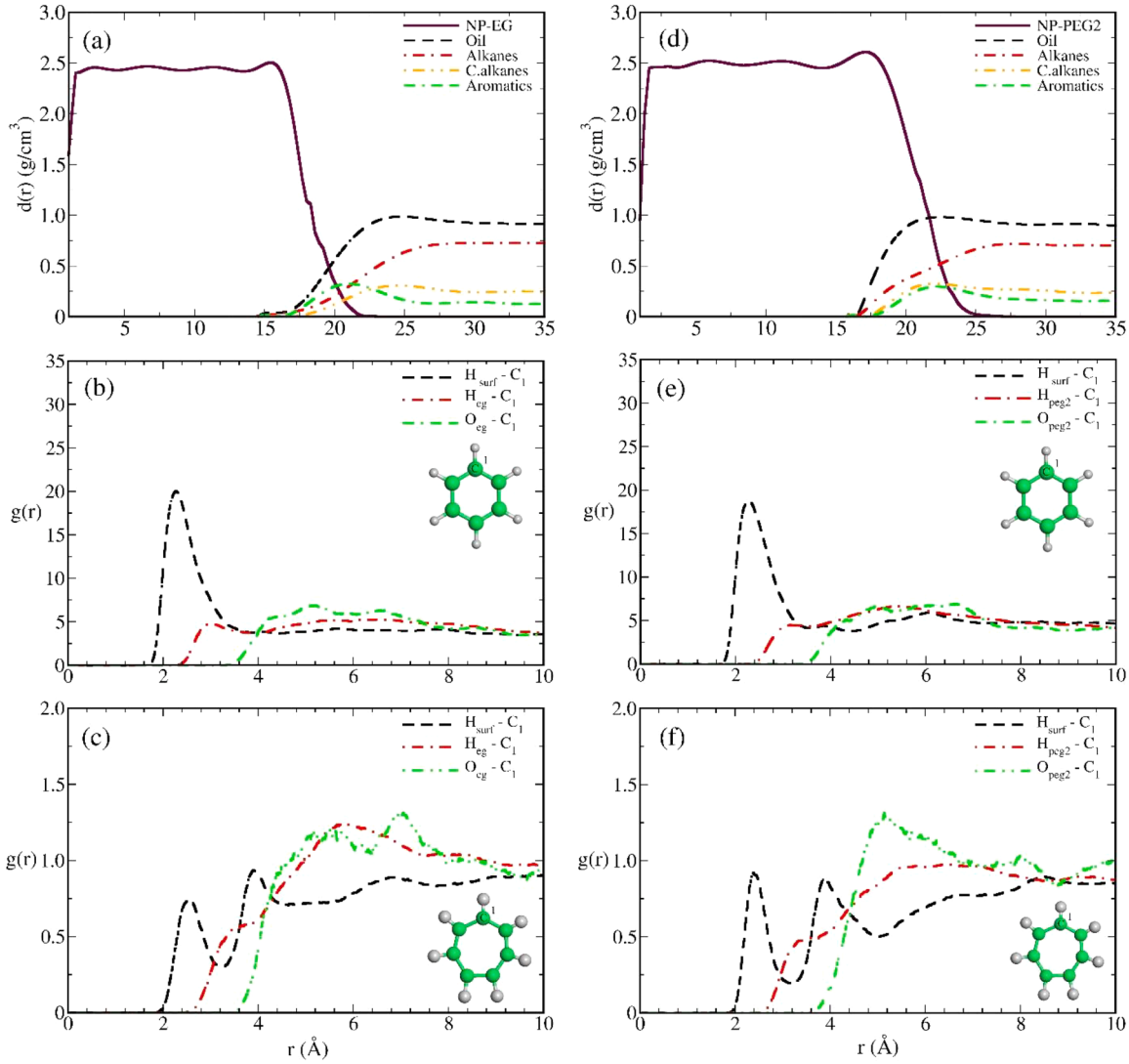

Fig. 3. (a) the density profile of hydrocarbons surrounding the NP, the radial pair distribution between selected atoms in the NP (see inset) and the carbon atoms in (b) benzene and (c) cycloheptane molecules for NP-EG–oil interfaces. Graphs (d)-(f) give the same results for the NP-PEG2–oil interfaces. All results correspond to a temperature of 300 K.

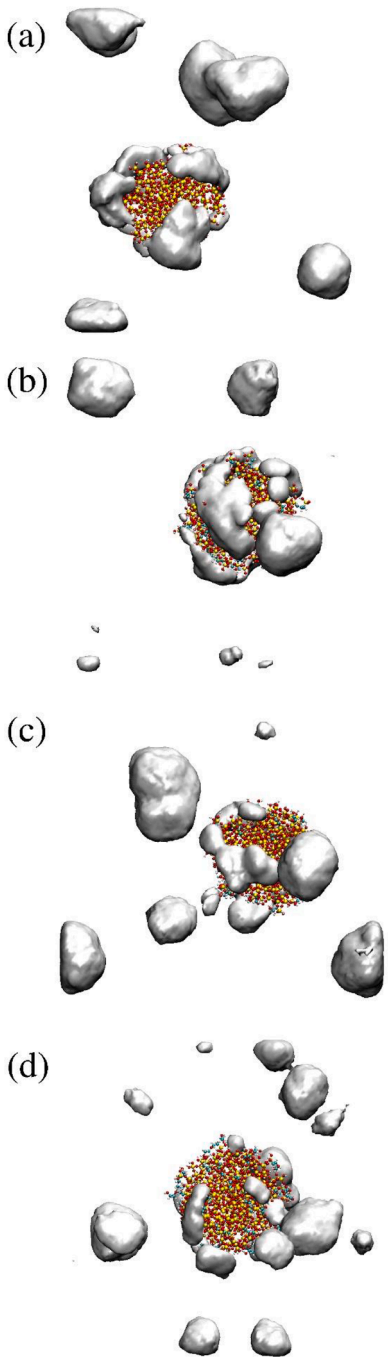

Fig. 4. Time-averaged distribution of benzene molecules on (a) NP-H, (b) NP-SA, (c) NP-EG, and (d) NP-PEG2 evaluated at 300 K and 1 atm. The positions are averaged over 2 ns for each system. The isovalues correspond to 0.18 g/cm^3.

(r) results, the accumulations of benzene molecules on NP-H (Fig. 4a) and NP-SA (Fig. 4b) are larger than on NP-EG (Fig. 4c) and NP-PEG2 (Fig. 4d). The visual accumulation of aromatic molecules on NP-H (Fig. 4a) and NP-SA (Fig. 4b) is almost equivalent for these two systems, primarily because both surface terminations are nonpolar [45].

An interesting result observed in Fig. 4a-d is that the benzene molecules accumulate non-homogeneously on NPs. These patchy aromatic domains were first observed in a brine–NP–oil interface by Lara *et al.* [10], where this effect can reduce the stability of NPs located at fluid–fluid interfaces [46]. From a qualitative comparison of the NPs evaluated in Fig. 4a-d, the NP-H surface provides more intense nucleation of aromatic molecules surrounding the nanoparticle surface.

Table 1
Density of benzene molecules surrounding the nanoparticle systems up to 27 Å from the nanoparticle center of mass.

Nanoparticle	Benzene (g/cm^3)
300 K	
NP-H	0.223
NP-SA	0.192
NP-EG	0.173
NP-PEG2	0.168
350 K	
NP-H	0.203
NP-SA	0.172
NP-EG	0.156
NP-PEG2	0.149

To quantify the accumulation of aromatic molecules on NPs, the density of benzene molecules surrounding each NP is presented in Table 1. The results show that the total density of molecules increases close to the NPs, compared to the partial density of benzene in the oil-only model (0.18 g/cm^3). A more significant nucleation of benzene molecules surrounds the NP-H surface. Compared to pristine oil, the density of benzene surrounding the NP-H increases by approximately 24% and 13% at 300 and 350 K, respectively. The tendency of aromatic molecules to accumulate decreases in the following order: NP-H, NP-SA, NP-EG, and NP-PEG2.

As seen in Fig. 4a-d, benzene molecules also form dispersed clusters in the oil phase. For benzene only, recent molecular simulations show that clusters of 13, 16, 19, and 23 molecules are more stable [28]. Although the exact magic numbers differ in the literature [25–28], all previous studies agree that the 13-molecule cluster is the most stable. For a multicomponent crude oil, experimental NMR measurements for three fossil fuel samples had an average value of 14, 15, and 20 aromatic molecules per cluster [25]. Based on the results given here, this is the first time that such clusters have been identified in a model multicomponent light crude oil containing a variety of aromatic molecules, alkanes, and cycloalkanes in the presence of NPs. Fig. 5 shows the number of clusters with a given number of benzene molecules (n) for all systems evaluated. Clusters with n = 9 and 11 molecules are the most frequently encountered during the simulations.

3.2. Transport and interfacial tension properties

The diffusion coefficients for the evaluated NPs-oil systems appear in Fig. 6. The diffusion coefficient changes with the temperature (300 and 350 K). However, this dependence is different for each NP. For example, the diffusion coefficients of NP-EG at 300 and 350 K differ by approximately 17%. The same result occurs for NP-PEG2. In contrast, the diffusion coefficient for NP-H at 350 K is ~9% greater than at 300 K. For NP-SA in oil, the diffusion changes by just ~4% between temperatures. At 300 K, the NP-H NP shows the largest diffusion coefficient for NPs within the oil. However, at 350 K, the NP-PEG2 shows the largest diffusion coefficient among the systems tested.

Fig. 7 shows the nanoparticle–oil interfacial tension (γ) for all systems. The temperature effects in γ are almost systematic for every sample. Notably, the NP-H–oil interfaces reduce interfacial tension by ~100 mN/m compared to other systems. The lower values of γ for oil–nanoparticles (together with their higher mobility) in NP-H–oil can be used in EOR through the structural disjoining pressure mechanism [12, 29]. With this technique, the NPs located at the intersection of the three phases can interact with oil, and a low oil–nanofluid interfacial tension is desirable. Additionally, the greater accumulation of benzene clusters on NP-H results in lower NP-H–oil interfacial tensions.

The values of γ for NP-H–oil at 300 and 350 K are approximately 0.913 N/m and 0.903 N/m, respectively. A similar result has been observed for a silica NP in an aqueous solution [7], where the hydroxyls

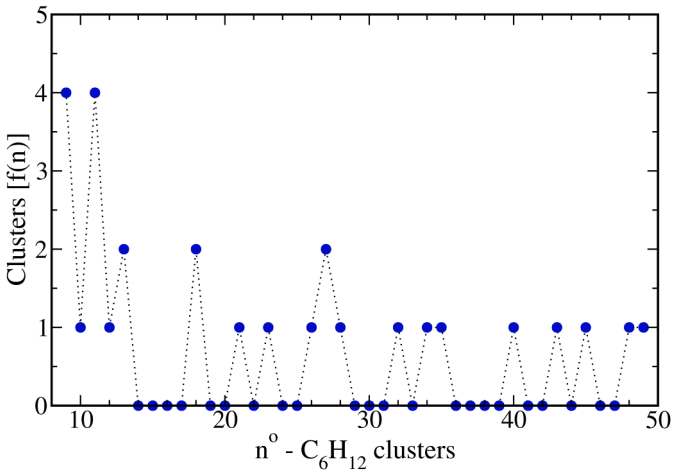

Fig. 5. Number of clusters with a given number of benzene molecules for all NPs-oil systems at 300 K.

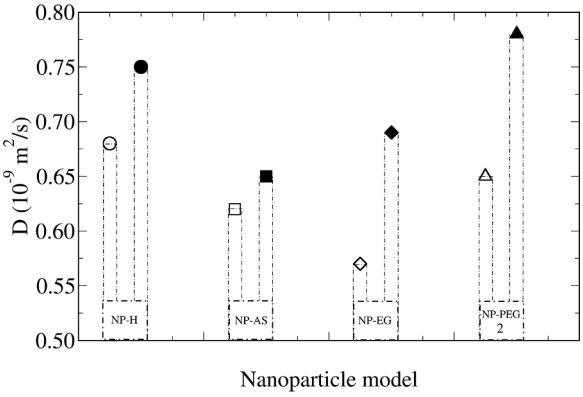

Fig. 6. Diffusion coefficient for evaluated nanoparticles within oil. Empty and full symbols represent values obtained at 300 K and 350 K, respectively.

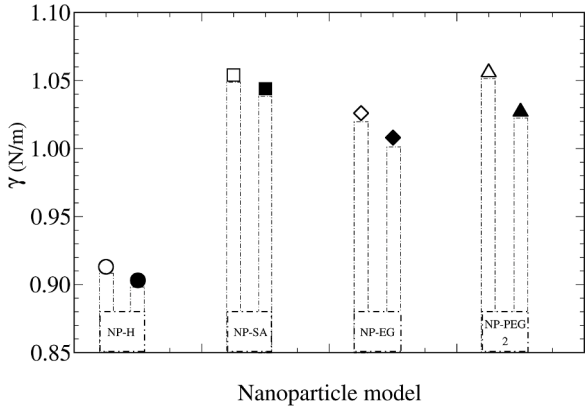

Fig. 7. Interfacial tension for nanoparticles within oil at 300 K (empty symbols) and 350 K (full symbols).

on the NP surface result in a greater affinity with water. In the same study, the presence of salt (NaCl and $CaCl_2$) in aqueous solutions has been shown to modify the surface properties of NPs, leading to changes in the interfacial tension values as the salt concentration in the solution increased. Earlier studies have also reported that the accumulation of aromatic molecules at the oil–water interface decreased interfacial tension [6,10,30]. This study found that the surface properties of NPs are modified by the accumulation of benzenes, which results in lower interfacial tension values for NP-H–oil interfaces compared to other systems studied here.

The interfacial tension data (γ) for the NP-EG and NP-PEG2 systems provide information regarding the effect of the PEG chain length. The NP-PEG2 system shows a γ that is 30 mN/m larger than NP-EG. This suggests that the chain length (and the corresponding intermolecular interactions between the hydrocarbons and the PEG spacers) leads to variations in the interfacial tension.

Conclusions

Fully atomistic molecular dynamics simulations were applied to evaluate silica nanoparticles covered by different functional groups dispersed in a model multicomponent light crude oil at different temperatures (300 and 350 K). The oil accumulations on the nanoparticles were evaluated, and the density profiles, interfacial tension, and diffusion coefficient were obtained.

i. Benzene molecules formed stable clusters dispersed in oil. Consistent with previous studies, clusters with 9 and 11 molecules appeared more frequently.

ii. The density profile analysis showed an accumulation of clusters of benzene molecules on the NP surfaces.

iii. The agglomeration of benzene clusters was larger for the hydroxylated nanoparticles (NP-H), where the hydrocarbons form a first shell of molecules ~25 Å in width, with a benzene density 24% greater than pristine oil.

iv. The density of benzene molecules in the first shell of aromatic molecules surrounding the NPs decreased in the order NP-H, NP-SA, NP-EG, and NP-PEG2.

v. Concerning the mobility of NPs, this study found that surface covering and temperature did not strongly affect the diffusion coefficient.

vi. The NP–oil interfacial tension values for NP-H show a significant decrease (approximately 15%) compared to other coverings (NP-SA, NP-EG, and NP-PEG2). This is consistent with the larger number of benzene clusters on the NP-H surface, demonstrating a benzene cluster size effect on the interfacial tension. Thus, controlling the affinity of nanoparticles with benzene clusters becomes a possible mechanism for tuning the NP–oil interfacial tension. The degree of this control is of central importance to applications in enhanced oil recovery using nanoparticles.

Declaration of Competing Interest

The authors declare that they have no known competing financial interests or personal relationships that could have appeared to influence the work reported in this paper.

Data availability

Data will be made available on request.
Data will be made available on request.

Acknowledgments

This work was supported by the Advanced Energy Consortium: http://www.beg.utexas.edu/aec/ Member companies include BP America Inc., BG Group, Petrobras, Repsol, Schlumberger, Statoil, Shell, and Total. The authors also acknowledge the financial support provided by the Brazilian agencies CAPES, CNPq, and Fapesp, the computational support from CENAPAD/SP, UFABC, UTFPR-CP and UTFPR-PG as well.

Supplementary materials

Supplementary material associated with this article can be found, in the online version, at doi:10.1016/j.susc.2023.122283.

References

[1] Y.-.S. Lin, K.R. Hurley, C.L. Haynes, J. Phys. Chem. Lett. 3 (2012) 364.
[2] I.I. Slowing, B.G. Trewyn, S. Giri, V.S.-Y. Lin, Adv. Funct. Mater. 17 (2007) 1225.
[3] L. Zhao, A. Seth, N. Wibowo, C.-.X. Zhao, N. Mitter, Y. Chengzhong, A.P. J. Middelberg, Vaccine 32 (2014) 327.
[4] H. Ogihara, J. Xie, J. Okagaki, T. Saji, Langmuir 28 (2012) 4605.
[5] B.W. Ewers, J.D. Batteas, J. Phys. Chem. C 48 (2012) 25165.
[6] L.S. de Lara, M.F. Michelon, C.R. Miranda, J. Phys. Chem. B 116 (2012) 14667.
[7] L.S. de Lara, M.F. Michelon, C.O. Metin, Q.P. Nguyen, C.R. Miranda, J. Chem. Phys. 136 (2012), 164702.
[8] L.S. de Lara, V.A. Rigo, M.F. Michelon, C.O. Metin, Q.P. Nguyen, C.R. Miranda, J. Phys.: Condens. Matter 27 (2015), 325101.
[9] L.S. de Lara, V.A. Rigo, C.R. Miranda, Eur. Phys. J. B 88 (2015) 261.
[10] L.S. de Lara, V.A. Rigo, C.R. Miranda, J. Phys. Chem. C 120 (2016) 6787.
[11] C.O. Metin, J.R. Baran Jr., Q.P. Nguyen, J. Nanopart. Res. 14 (2012) 1246.
[12] H. Zhang, A. Nikolov, D. Wasan, Energy Fuels 28 (2014) 3002.
[13] A.J. Worthen, L.M. Foster, J. Dong, J.A. Bollinger, A.H. Peterman, L.E. Pastora, S. L. Bryant, T.M. Truskett, C.W. Bielawski, K.P. Johnston, Langmuir 30 (2014) 984.
[14] E. Akhayere, D. Kavaz, A. Vaseashta, Appl. Sci. 12 (2022) 9279.
[15] J. Lyklema, *Adv. Colloid and Interface Sci.* **147-148**, 205 (2009); A. Dukhin, S. Dukhin, P. Goetz, Langmuir 21 (2005) 9990.
[16] A. Dukhin, S. Dukhin, P. Goetz, Langmuir 21 (2005) 9990.
[17] J. Lyklema, Fundamentals in Colloid and Interface Science, Vol. II, Academic Press, New York, 1995.
[18] V.A. Rigo, L.S. de Lara, C.R. Miranda, Appl. Sur. Sci. 292 (2014) 742.
[19] Z. Zhang, A.E. Berns, S. Willbold, J. Buitenhuis, *J. Colloid Interface Sci.* **310**, 446 (2007); J.M.D. Lane, A.E. Ismail, M. Chandross, C.D. Lorenz, G.S. Grest, Phys. Rev. E 79 (R) (2009) 050501.
[20] J.M.D. Lane, A.E. Ismail, M. Chandross, C.D. Lorenz, G.S. Grest, *Phys. Rev. E* **79**, 050501(R) (2009); M. Ledyastuti, Y. Liang, M. Kunieda, T. Matsuoka, J. Chem. Phys. 137 (2012) 064703.
[21] M. Ledyastuti, Y. Liang, M. Kunieda, T. Matsuoka, *J. Chem. Phys.* **137**, 064703 (2012); B. Coasne, J.T. Fourkas, J. Phys. Chem. C 115, 15471 (2011).
[22] B. Coasne, J.T. Fourkas, *J. Phys. Chem. C* **115**, 15471 (2011); H. Fan, D.E. Resasco, A. Striolo, Langmuir 27 (2011) 5264.
[23] H. Fan, D.E. Resasco, A. Striolo, *Langmuir* **27**, 5264 (2011); L. Parolini, A.D. Law, A. Maestro, D.M.A. Buzza, P. Cicuta, J. Phys.: Condens. Matter 27 (2015) 194119.
[24] L. Parolini, A.D. Law, A. Maestro, D.M.A. Buzza, P. Cicuta, *J. Phys.: Condens. Matter* **27**, 194119 (2015); K. Mao, G.J. Kennedy, S.M. Althaus, M. Pruski, Energy Fuels 27 (2013) 760.
[25] K. Mao, G.J. Kennedy, S.M. Althaus, M. Pruski, *Energy Fuels* **27**, 760 (2013); H. Takeuchi, J. Phys. Chem. A 116 (2012) 10172.
[26] H. Takeuchi, *J. Phys. Chem. A* **116**, 10172 (2012); C.-.F. Fu, S.X. Tian, J. Chem. Theory Comput. 7 (2011) 2240.
[27] C.-F. Fu, S.X. Tian, *J. Chem. Theory Comput.* **7**, 2240 (2011); M. Bartolomei, F. Pirani, J.M.C. Marques, J. Comput. Chem. 36 (2015) 2291.
[28] M. Bartolomei, F. Pirani, J.M.C. Marques, *J. Comput. Chem.* **36**, 2291 (2015); D.T. Wasan, A.D. Nikolov, Nature 423 (2003) 156.
[29] D.T. Wasan, A.D. Nikolov, *Nature* **423**, 156 (2003); M. Kunieda, K. Nakaoka, Y. Liang, C.R. Miranda, A. Ueda, S. Takahashi, H. Okabe, T. Matsuoka, J. Am. Chem. Soc. 132 (2010) 18281.
[30] M. Kunieda, K. Nakaoka, Y. Liang, C.R. Miranda, A. Ueda, S. Takahashi, H. Okabe, T. Matsuoka, *J. Am. Chem. Soc.* **132**, 18281 (2010); J.S. de Almeida, C.R. Miranda, Sci. Rep. 6 (2016) 28128.
[31] J.S. de Almeida, C.R. Miranda, *Scientific Reports*, **6**, 28128 (2016); L.T. Zhuravlev, Colloids Surf. A: Physicochem. Eng. Aspects 173 (2000) 1.
[32] L.T. Zhuravlev, Colloids and Surfaces A*: Physicochem. Eng. Aspects* **173**, 1 (2000); D. Makimura, C. Metin, T. Kabashima, T. Matsuoka, Q.P. Nguyen, C.R. Miranda, J. Mater Sci. 45 (2010) 5084.
[33] D. Makimura, C. Metin, T. Kabashima, T. Matsuoka, Q.P. Nguyen, C.R. Miranda, *J. Mater Sci.* **45**, 5084 (2010); A.P. Thompson, S.J. Plimpton, W. Mattson, J. Chem. Phys. 131 (2009) 154107.
[34] A.P. Thompson, S.J. Plimpton, W. Mattson, *J. Chem. Phys.* **131**, 154107 (2009); B. R. Brooks, C.L. Brooks III., A.D. Mackerell Jr., L. Nilsson, R.J. Petrella, B. Roux, Y. Won, G. Archontis, C. Bartels, S. Boresch, et al., J. Comput. Chem. 30 (2009) 1545.
[35] B.R. Brooks, C.L.III. Brooks, A.D.Jr. Mackerell, L. Nilsson, R.J. Petrella, B. Roux, Y. Won, G. Archontis, C. Bartels, S. Boresch, et al., J. Comput. Chem. 30 (2009) 1545.
[36] E.R. Cruz-Chu, A. Aksimentiev, K. Schulten, *J. Phys. Chem. B* **110**, 21497 (2006); R. W. Hockney, J.W. Eastwood, Computer Simulation using Particles, Adam Hilger, New York, 1989.
[37] R.W. Hockney, J.W. Eastwood, in *Computer Simulation using Particles* (Adam Hilger: New York, 1989); S. Nosé, J. Chem. Phys. 81 (1984) 511.
[38] S. Nosé, *J. Chem. Phys.* **81**, 511 (1984)W.G. Hoover, Phys. Rev. A: At., Mol., Opt. Phys. 31 (1985) 1695.
[39] W.G. Hoover, *Phys. Rev. A: At., Mol., Opt. Phys.* **31**, 1695 (1985); H.C. Andersen, J. Chem. Phys. 72 (1980) 2384.
[40] H.C. Andersen, *J. Chem. Phys.* **72**, 2384 (1980) I.V. Schweigert, K.E.J. Lehtinen, M. J. Carrier, M.R. Zachariah, Phys. Rev. B: Condens. Matter Mater. Phys. 65 (2002) 235410.
[41] I.V. Schweigert, K.E.J. Lehtinen, M.J. Carrier, M.R. Zachariah, *Phys. Rev. B: Condens. Matter Mater. Phys.* **65**, 235410 (2002); T. Hawa, M.R. Zachariah, J. Chem. Phys. 121 (2004) 9043.
[42] T. Hawa, M.R. Zachariah, *J. Chem. Phys.* **121**, 9043 (2004); S.M. Thompson, K.E. Gubbins, J.P.R.B. Walton, R.A.R. Chantry, J.S. Rawlinson, J. Chem. Phys. 81 (1984) 530.
[43] S.M. Thompson, K.E. Gubbins, J.P.R.B. Walton, R.A.R. Chantry, J.S. Rawlinson, *J. Chem. Phys.* **81**, 530 (1984); B. Coasne, J.T. Fourkas, J. Phys. Chem. C 115 (2011) 15471.
[44] B. Coasne, J.T. Fourkas, *J. Phys. Chem. C* **115**, 15471 (2011); K.J. Williamson, Macroscale and Microscale Organic Experiments, D. C. Heath, Lexington, 1994.
[45] K.J. Williamson, *Macroscale and Microscale Organic Experiments*, Phys. Rev. E 74 (2006), 021406.
[46] W. Chen, S. Tan, Z. Huang, T.-K. Ng, W.T. Ford, P. Tong, *Phys. Rev. E* **74**, 021406 (2006); E. Akhayere, D. Kavaz., A. Vaseashta, Appl. Sci. 12 (2022) 9279.